Journal of Non-Crystalline Solids 120 (1990) 275–282
North-Holland

Aeg 731

STRUCTURAL DIFFERENCE OF SURFACE AND SUB-SURFACE NATIVE OXIDES OF EVAPORATED AMORPHOUS SILICON

Masato TADA

Osaka Prefectural College of Technology, Saiwai-cho, Neyagawa, Osaka 572, Japan

Hisashi OHSAKI and Michel André AEGERTER

Instituto de Fisica e Quimica de São Carlos, Universidade de São Paulo, Sao Carlos (SP), Brazil

Evaporated amorphous silicon (a-Si) films, oxidized in air or O_2 at room temperature, present two native oxides with different structures. The surface oxide is constructed from SiO_4-tetrahedron structural units with a 110° O–Si–O angle, which is the common structural unit of stable silicon oxides. The internal oxide has a different structure having a 120° O–Si–O angle. The results of molecular orbital (MO) calculations for $(SiO_3)^{m-}$ and $(SiO_4)^{n-}$ anionic clusters support the presence of the two stable structures of silicon oxides and also reveal the importance of the ionic character of the oxidized sites.

1. Introduction

It is well known that amorphous materials have a medium range order (up to 15 Å) with the atoms widely distributed around the average sites. The experimental techniques available to characterize this intermediate range order do not give explicit results and it is difficult to separate the nature of the network of the surface from that of the bulk.

In this work, structural analyses by electron diffraction of very thin oxidized a-Si films (thickness of 5–80 Å) provide precise information about the native oxides produced at the surface and at the inside of an a-Si film by the oxidation process. As the a-Si network limits the displacements of the reacting atoms, the structure of both oxides is not necessarily the same as that resulting from liquid- or gas-phase oxidations. We discuss the role of the a-Si network on the oxidation process and the formation mechanism of the surface and internal oxides. Moreover, ab initio MO calculations for anionic clusters of the type $(SiO_3)^{m-}$ and $(SiO_4)^{n-}$ support the presence of two different oxides observed experimentally and also reveal the importance of the ionic character of the oxidized sites.

2. Experimental

Amorphous silicon films were prepared by electron-beam evaporation of silicon single crystals having a specific resistance of 5 Ω cm. The substrates were thin films of nitrocellulose placed on #100 Cu mesh grids, and they were thoroughly degassed by heating in order to obtain homogeneous a-Si films without cracks or pores [1,2]. During the deposition, the temperature of the substrates was maintained between 20 and 50 °C. The film thickness of a-Si was controlled with an accuracy of ±1 Å by using a calibrated quartz oscillator [3]. After the deposition, the a-Si films were placed in a dessicator, which was evacuated and rinsed several times with pure oxygen gas at atmospheric pressure and at room temperature. After oxidation, the nitrocellulose substrate was dissolved in isoamyl acetate to obtain a substrate-free film sample on the Cu mesh grid.

An electron diffraction system with an r^3-sector [4] and an electron-beam size of about 70 μm was operated at an electron energy of 55.8 keV. The diffraction pattern of the oxidized a-Si films was measured in the s-value range 0.5 to 30 $Å^{-1}$, where $s = (4\pi/\lambda)\sin(\theta/2)$, θ being the angle be-

0022-3093/90/$03.50 © 1990 – Elsevier Science Publishers B.V. (North-Holland)

tween the incident and diffracted beams, and λ the electron wavelength. The radial distribution functions (RDF) were obtained from the diffraction data by using the sine Fourier transformation method [5,6]. In order to obtain RDF curves with the highest possible resolution, no artificial temperature factor has been used in the transformation procedure.

The growth mechanism of the oxides was also studied by calculating the ab initio self-consistent-field MO of anionic clusters such as $(SiO_3)^{m-}$ ($m = 0, 1, 2$ and 3) and $(SiO_4)^{n-}$ ($n = 0, 1, 2, 3$ and 4) using a STO-3G basis and the computer program GAUSSIAN-80 [7].

3. Results and discussion

The interatomic interference scattering intensity is obtained from the diffraction data following a procedure already described in refs. [5] and [6]. The interference functions $s \cdot M(s)$ for 80, 40 and 20 Å thick a-Si films exposed to oxygen gas during periods of 3, 3 and 1 weeks, respectively, are shown in fig. 1; the reduced RDF curves are presented in fig. 2. For the RDF calculation we used only the solid line part of the interference functions in fig. 1 because the finite integrand at the terminal point of the integration induces undesirable ripples. The assignment of most of the

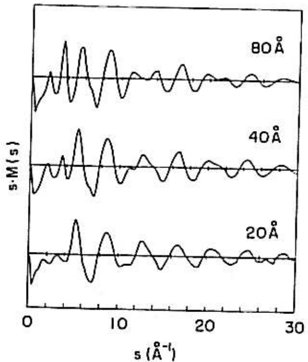

Fig. 1. Interference functions $s \cdot M(s)$ versus s of oxidized a-Si films with 80, 40 and 20 Å thicknesses.

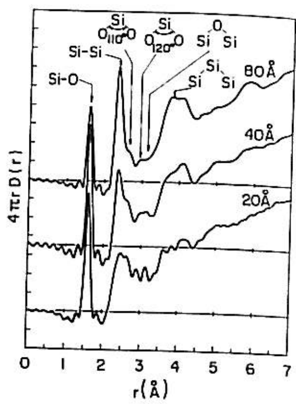

Fig. 2. Radial distribution functions of oxidized a-Si films with 80, 40 and 20 Å thicknesses.

peaks is already well established in the literature. From the similarity to the Si–Si atomic distances of c-Si, the peaks at 2.36 and 3.85 Å are attributed to Si–Si atomic pairs of the a-Si network in the first and second neighbors configurations, respectively. From the analogy of the atomic distances for stable silicon oxides such as crystalline SiO_2 [8–14], vitreous silica [15–17] and silicon monoxide [18,19], the peaks at 1.6, 2.6 and 3.2 Å can be assigned to Si–O bonded pairs, O–Si–O pairs with 110° O–Si–O angle, and Si–O–Si atomic pairs, respectively. By using an artificial damping factor which eliminates the ripples present on both sides of real atomic peaks without changing their positions, the small peak at 2.9 Å was found to be real and was attributed to the O–Si–O atomic pair having an angle of about 120° [6]. The assignment of the peak to a Si–O–Si atomic pair is discarded since all the stable silicon oxides have Si–Si distances larger than 3.0 Å.

The relative peak-height of the 110° O–Si–O atomic pair increases when the film thickness decreases, but the peak of the 120° O–Si–O atomic pair does not show the same dependence. High resolution transmission electron micrographs with a resolution down to 15 Å show that the a-Si films are homogeneous and without cracks and pores [1]. The fact that self-supported 5 Å thick films have been obtained (see below) indicates that the

atomic network is continuous down to this scale and does not consist of particles or grains. Therefore, we assume that all the films deposited under the same experimental condition (environmental pressure, deposition rate, substrate temperature, etc) exhibit the same homogeneity and uniformity. Consequently, both structures are thought to originate at different oxidation sites. The oxide with a 110° angle structure is derived from a surface oxide layer having a constant thickness, independent of the film thickness. The oxide with a 120° angle structure is, however, distributed uniformly in the film [1,20]. The distribution of these two oxides is confirmed by the results obtained with an extremely thin a-Si film (5 Å thickness) oxidized in pure O_2 gas for 6 months. Its interference function is shown in fig. 3 and the reduced RDF curve is given in the lower part of fig. 4. The Si–Si peak no longer appears around 2.36 Å, and consequently all the Si–Si bonds were broken during the oxidation. The upper part of fig. 4 shows a least squares fit of the respective contribution of Si–O atomic pairs and 110° O–Si–O atomic pairs to the reduced RDF. Analyzing the residual RDF (plain curve), we see that the Si–O–Si peak at 3.2 Å has a small shoulder at the same position as that of the 120° O–Si–O peak. Thus, a small amount of internal oxide with 120° O–Si–O structure is also present in the film together with the surface oxide with the 110° O–Si–O structure. Consequently, as both oxides are present in this film and as the Si–Si bond

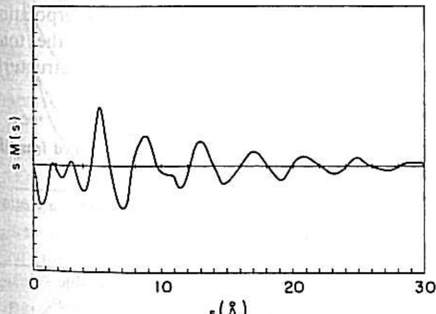

Fig. 3. Interference function $s \cdot M(s)$ versus s of oxidized a-Si film with 5 Å thickness.

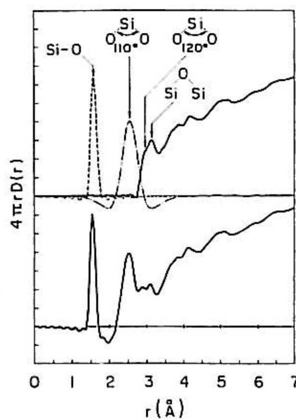

Fig. 4. The lower part shows the radial distribution function of oxidized a-Si film with 5 Å thickness. The upper part shows a peak fit to the Si–O atomic pairs (dashed line) and 110° O–Si–O atomic pairs (two dotted line). The plain curve is the residual RDF curve.

length of the a-Si network is about 2.36 Å, we can conclude that the surface oxide with the 110° O–Si–O structure is only formed with Si atoms of the first or second silicon surface layer.

One possible cause of the difference in the structure of the surface and the internal oxides is the differences in ease of the displacements of Si atoms in the atomic network during the oxidation process. The principal features of the oxidation process are the breaking of Si–Si bonds and the separation of the Si atoms by the inserted O atom. The distance between the Si atoms is therefore changed from 2.36 Å (Si–Si bond) to 3.2 Å for the Si–O–Si bridging structure. The Si atoms on the surface can be easily displaced and will prefer to bond to four O atoms. On the other hand, the Si atoms inside the film will not easily bond to O atoms because of their limited displacement in the atomic network. Accordingly, the surface oxide is composed of stable SiO_4-tetrahedrons with a 110° O–Si–O angle and the internal oxide has a different structure with a 120° O–Si–O angle.

The UV-light irradiation experiment also confirms the cause of the difference in the oxide structure. An 80 Å thick a-Si film was oxidized in an O_2 gas environment for 6 months; after this

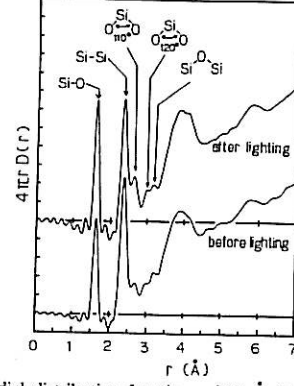

Fig. 5. Radial distribution functions of 80 Å thick a-Si film before and after exposure to UV light.

period of exposure, there is no further oxidation [1,20]. The film was then exposed to the UV-light of a 150 W Xe-short-arc lamp with about 50 mW/cm^2 for 5 h. The reduced RDF curves for the film unexposed and exposed to the UV-light are shown in fig. 5. The curves show that the irradiation causes three changes on the RDF: (i) an increase of the Si–O peak height, (ii) a decrease of the Si–Si peak height, and (iii) an increase of the 110° O–Si–O peak height. The first two changes indicate that the UV-light allows further oxidation of the a-Si film. Therefore, the increase of the amount of the oxide with the SiO_4-tetrahedron structure originates from the additional oxidation rather than from the reconstruction of the internal oxide having a 120° O–Si–O angle structure. As the surface of a-Si is already satisfied, the additional oxide is likely to be produced at or below the interface between the native surface oxide

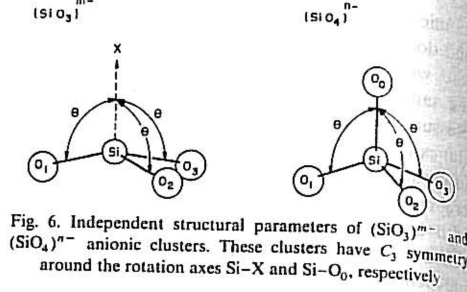

Fig. 6. Independent structural parameters of $(SiO_3)^{m-}$ and $(SiO_4)^{n-}$ anionic clusters. These clusters have C_3 symmetry around the rotation axes Si–X and Si–O_0, respectively.

layer and the a-Si network. This increase probably results from the vibrations of the Si network produced by the UV-light, because the UV photons are only absorbed by the a-Si and not by the silicon oxide [21].

In order to obtain information concerning the stability and the reactivity of the two oxide structures, we made ab initio chemical computations for anionic SiO_3 and SiO_4 clusters. We assumed that each cluster has a C_3 symmetry and two independent structural parameters: the Si–O distance r_{Si-O} and the angle as shown in fig. 6. Since the oxidation site is not necessarily neutral and may contain atom(s) with dangling bond(s) during the reaction, the oxygen atoms of the clusters are not terminated.

The structural parameters of the optimized structure for each cluster having a minimum total-energy are listed in tables 1 and 2. The status column gives the stability of the clusters. This status was inspected from the total-energy curves drawn by using four points Legendre interpolation and extrapolation from the values of the total energy of each cluster with various structural

Table 1
Optimized structural parameters of $(SiO_3)^{m-}$ clusters. The status column shows the cluster stability which is determined from the curves for the total energy of the cluster against the Si–O distance r_{Si-O} and the angle θ.

Ionicity	Si–O distance (Å)	θ	Energy (Hartree)	Electron population		Status
				Si	O	
0	1.6239	99.10°	−506.768117	13.08	8.23–8.35	unstable
−1	1.6140	90.00°	−506.843213	13.29	8.42–8.64	unstable
−2	1.6121	90.00°	−506.387954	13.49	8.84	stable
−3	1.7595	109.30°	−505.562305	14.17	8.94	stable

Table 2
Optimized structural parameters of $(SiO_4)^{n-}$ clusters. The status column shows the cluster stability which is determined from the curves for the total energy of the cluster against the Si–O distance r_{Si-O} and the angle θ

Ionicity	Si–O distance (Å)	θ	Energy (Hartree)	Electron population		Status
				Si	O	
0	–	–	–	–	–	cannot be optimized
−1	1.6986	107.43°	−580.676623	13.13	8.38–8.56	unstable
−2	1.6873	104.92°	−580.055331	13.37	8.51–8.71	unstable
−3	1.7471	101.77°	−579.554593	13.59	8.59–8.95	unstable
−4	1.7969	109.47°	−578.550672	13.81	9.05	stable

parameters. The SiO_3 cluster has two stable structures with electronegativities 2 and 3; the total-energy surfaces versus r_{Si-O} or θ are shown in figs. 7 and 8. Figure 9 shows that the SiO_4 cluster has a stable structure with an electronegativity of 4. On the other hand, we could not get any optimized structure for neutral SiO_4 clusters using the Gaussian 80 program [7]. The total energy of the tetrahedral $(SiO_4)^0$ cluster with θ being 109.47° was first calculated with varying r_{Si-O} (fig. 10). The curve shows an energy minimum at $r_{Si-O} = 1.677$ Å. However, the total-energy calculations for an $(SiO_4)^0$ cluster having $r_{Si-O} = 1.670$ Å, near the energy minimum point, shows several dips on the energy surface (fig. 11). This indicates that the neutral SiO_4 cluster is unstable. $(SiO_3)^{m-}$ with $m = 0$ and 1 and $(SiO_4)^{n-}$ with $n = 1$, 2 and 3 have a similar behaviour, and we also consider that they are unstable clusters.

MO calculations show that the SiO_3 cluster has two stable structures: a $(SiO_3)^{2-}$ planar structure

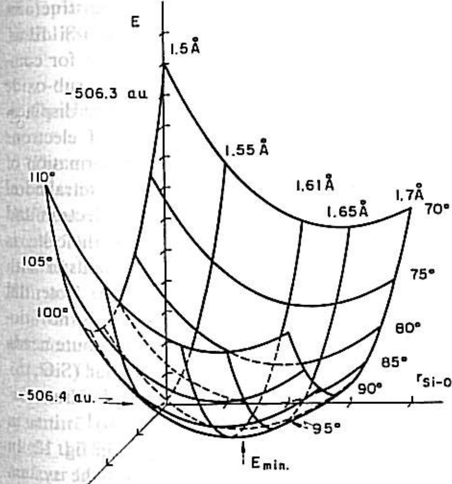

Fig. 7. Total-energy surface of $(SiO_3)^{2-}$ cluster.

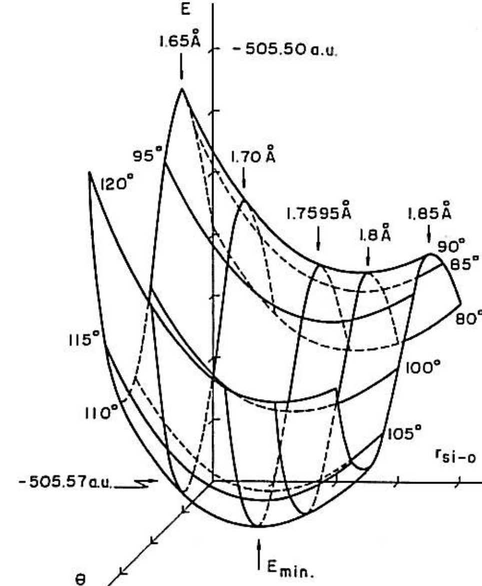

Fig. 8. Total-energy surface of $(SiO_3)^{3-}$ cluster.

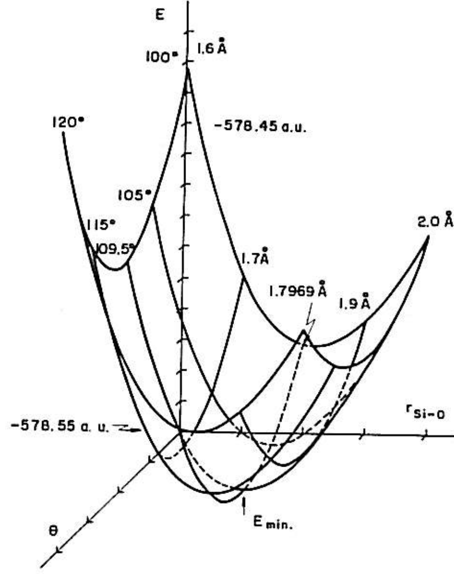

Fig. 9. Total-energy surface of $(SiO_4)^{4-}$ cluster.

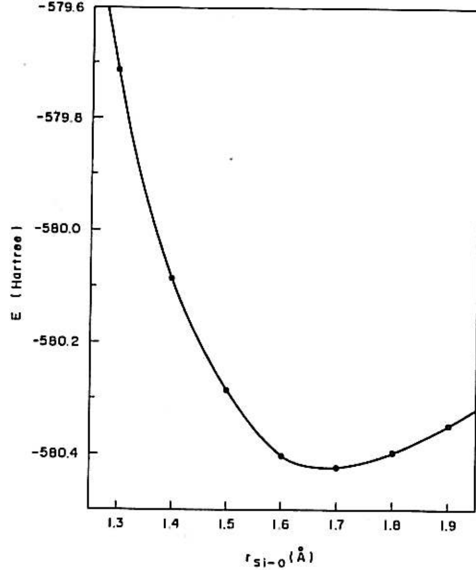

Fig. 10. Total energy of $(SiO_4)^0$ cluster with $\theta = 109.47°$ versus Si–O distance.

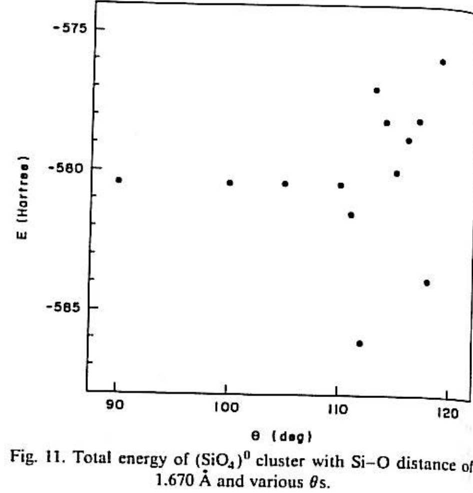

Fig. 11. Total energy of $(SiO_4)^0$ cluster with Si–O distance of 1.670 Å and various θs.

with $\theta = 90°$ and an 120° O–Si–O angle and a $(SiO_3)^{3-}$ pre-tetrahedral structure with $\theta = 110°$ and 110° O–Si–O angle. They also indicate that the SiO_4 cluster has only one stable structure, that is the tetrahedral $(SiO_4)^{4-}$. These results support the presence of the two different stable structures which are observed in the oxidized a-Si films. Moreover, there are two possible routes for completion of a tetrahedral SiO_4 unit from a sub-oxide SiO_3 cluster under the condition of free displacement of atoms and free movement of electrons during the oxidation: one is the transformation of a planar $(SiO_3)^{2-}$ cluster into a pre-tetrahedral $(SiO_3)^{3-}$ cluster by the capture of an electron and the following addition of one O^- ion; the other is a direct reaction of a planar $(SiO_3)^{2-}$ cluster with an O^{2-} ion. The first route has no potential barrier because the $(SiO_3)^{3-}$ cluster is not deformed. On the other hand, the second route needs a change in the geometry of the planar $(SiO_3)^{2-}$ cluster. The optimizing process for the transformation of a (planar $SiO_3 + O$ atom$)^{4-}$ into a tetrahedral $(SiO_4)^{4-}$ cluster is shown in fig. 12. In this calculation, it was assumed that the system has a C_3 symmetry similar to the $(SiO_3)^{m-}$ cluster shown in fig. 6 and that the additive O atom lies on the Si–X axis. The system is initially con-

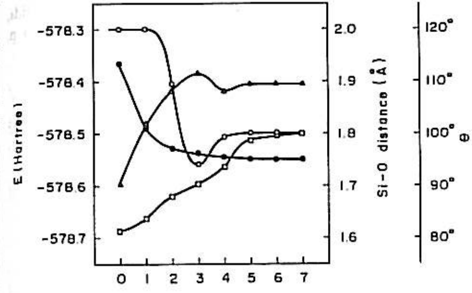

Fig. 12. Optimized transformation of a (planar $SiO_3 + O$ atom$)^{4-}$ into a tetrahedral $(SiO_4)^{4-}$ cluster. □, ○, △, ● represent the distance between Si atom and the additive O atom, the distance between the Si atom and O atoms belonging to the planar SiO_3 cluster, the angle between the bonds (additive O atom–Si atom) and (Si atom–O atoms belonging to the SiO_3 cluster), and the total energy, respectively.

structed from a SiO_3 cluster with structural parameters identical to those of the stable planar $(SiO_3)^{2-}$ cluster and a distant O atom. The system is deformed into a stable tetrahedral $(SiO_4)^{4-}$ cluster allowing a smooth decrease of the total energy. This result shows that the direct reaction of a planar $(SiO_3)^{2-}$ and O^{2-} ion into a tetrahedral $(SiO_4)^{4-}$ is possible.

4. Conclusions

The oxidation of a-Si film in air or O_2 gas at room temperature results in the formation of two different oxides: a surface oxide and an internal oxide. The surface oxide is generated by the oxidation of the first or second surface layer of the a-Si film and is composed of SiO_4-tetrahedron structural units with a 110° O–Si–O angle which are the common structural units of the stable silicon oxides. The internal oxide has a different structure with a 120° O–Si–O angle. The difference in the structure occurs from the difference of the oxidized sites: the Si atoms on the film surface bond easily to four O atoms as their displacements are easier; the Si atoms inside the film do not bond easily to O atoms because of the limited deformation of the Si network surrounding the Si atom.

The results of MO calculations support the presence of the two stable oxides with different structures. The SiO_3 cluster with an electronegativity of 2 has a stable structure with a 120° O–Si–O angle while the SiO_3 cluster with an electronegativity of 3 and the SiO_4 cluster with an electronegativity of 4 have a 110° O–Si–O structure. These results indicate that the ionic character of the oxidized site plays an important role in the structure of the oxide.

The authors are grateful to Professor T. Shichiri of Osaka City University for his useful suggestions. This work is partly supported by CNPq (Brazil).

References

[1] H. Ohsaki, K. Miura and Y. Tatsumi, J. Non-Cryst. Solids 93 (1987) 395.
[2] I. Ohdomari, M. Kakumu, H. Sugahara, M. Hori, T. Saito, T. Yonehara and Y. Hajimoto, J. Appl. Phys. 52 (1981) 6617.
[3] K. Miura, M. Tada, H. Ohsaki, S. Kodera and T. Ino, J. Non-Cryst. Solids 95&96 (1987) 1095.
[4] T. Ino, J. Phys. Soc. Jpn. 8 (1953) 92.
[5] H. Ohsaki and M. Tada, Jpn. J. Appl. Phys. 25 (1986) 1768.
[6] H. Ohsaki, K. Miura, Y. Tatsumi and T. Ino, Jpn. J. Appl. Phys. 25 (1986) 1773.
[7] J.S. Binkley, R.A. Whiteside, R. Krishman, R. Seeger, D.J. DeFrees, H.B. Schlegel, S. Topiol. L.R. Kahn and J.A. Pople, GAUSSIAN-80 An Ab-Initio Molecular Orbital Program, Department of Chemistry, Carnegie-Mellon University, Pittsburgh. PA.
[8] R.A. Young and D. Post, Acta Crystallogr. B15 (1962) 337.
[9] R.A. Young, Defense Doc. Contact USA Lep. (1962).
[10] A.F. Wright and J. Leadbetter, Philos. Mag. 31 (1975) 1391.
[11] D.R. Peacor, Z. Kristallogr. 138 (1973) 273.
[12] J.H. Konnert and D.E. Appleman, Acta Crystallogr. B34 (1978) 391.
[13] T. Zoltai and M.J. Buerger, Z. Kristallogr. 111 (1959) 129.
[14] J. Shorpshire, P.P. Keat and P.A. Bangham, Z. Kristallogr. 121 (1964) 369.
[15] R.L. Mozzi and B.E. Warren, J. Appl. Crystallogr. 2 (1969) 164.
[16] A.H. Narten, J. Chem. Phys. 56 (1972) 1905.
[17] J.H. Konnert and J. Karle, Acta Crystallogr. A29 (1973) 702.

[18] M.V. Coleman and D.J.D. Thomas, Phys. Status Solidi 22 (1967) 593.
[19] R. Engelke, Th.R.H.-G. Neuman and K. Hubner, Phys. Status Solidi A65 (1981) 271.
[20] H. Ohsaki, M.A. Aegerter and M. Tada, Phys. Rev. Lett., in press.
[21] D.F. Edwards, Handbook of Optical Constants of Soli[ds], ed. E.D. Palik (Academic Press, Orlando, FL, 1985) 547;
H.R. Philipp, ibid., p. 719.